Shape optimisation of air-cooled finned-tube heat exchangers

H. Nemati[1], M.A. Moghimi[2,*], P. Sapin[3], C.N. Markides[3]

[1] Department of Mechanics, Marvdasht Branch, Islamic Azad University, Marvdasht, Iran.
[2] Department of Design and Engineering, Staffordshire University, Stoke-On-Trent ST4 2DE, UK. * Corresponding author: Mohammad.Moghimi-Ardekni@staffs.ac.uk; moghimi64@gmail.com
[3] Clean Energy Processes (CEP) Laboratory, Department of Chemical Engineering, Imperial College London, South Kensington Campus, London SW7 2AZ, UK

Abstract

The use of annular fins in air-cooled heat exchangers is a well-known solution, commonly used in air-conditioning and heat-recovery systems, for enhancing the air-side heat transfer. Although associated with additional material and manufacturing costs, custom-designed finned-tube heat exchangers can be cost-effective. In this article, the shape of the annular fins in a multi-row air heat exchanger is optimised in order to enhance performance without incurring a manufacturing cost penalty. The air-side heat transfer, pressure drop and entropy generation in a regular, four-row heat exchanger are predicted using a steady-state turbulent CFD model and validated against experimental data. The validated simulation tool is then used to perform model-based optimisation of the fin shapes. The originality of the proposed approach lies in optimising the shape of each fin row individually, resulting in a non-homogenous custom bundle of tubes. Evidence of this local-optimisation potential is first provided by a short preliminary study, followed by four distinct optimisation studies (with four distinct objective functions), aimed at addressing the major problems faced by designers. Response-surface methods – namely, NLPQL for single-objective and MOGA for multi-objective optimisations – are used to determine the optimum configuration for each optimisation strategy. It is shown that elliptical annular-shaped fins minimise the pressure drop and entropy generation, while circular-shaped fins at the entrance region (i.e., first row) can be employed to maximise heat transfer. The results also show that, for the scenario in which the total heat transfer rate is maximised and the pressure drop minimised, the pressure drop is reduced by up to 31%, the fin weight is reduced up to 23 %, with as little as a 14 % decrease in the total air-side heat transfer, relative to the case in which all the fins across the tube bundle are circular. Moreover, in all optimised cases, the entropy generation rate is also reduced, which shows a thermodynamic improvement in tube bundle performance.

Keywords: Annular fins, Finned tube, Elliptical fin, CFD, Response surface optimisation, Multi-objectives optimisation, Single objective optimisation, Entropy generation minimisation.

1- Introduction

Space heating and industrial processes are two of the main engineering applications of air heat exchangers. These heat exchangers do not suffer the severe corrosion and leakage problems that are more common with liquid heat exchangers. In addition, these heaters are getting popular due to their cost-effectiveness and easy maintenance, and are often used in novel engineering applications based on renewable energy sources, such as solar air heaters [1-5] and zero energy

buildings [6, 7]. However, the main drawback of air heat exchangers is their low thermal performance due to the low air-side heat transfer coefficient (i.e., between the absorber and the air flow). A popular suggested solution for these heat exchangers is using extended surfaces or fins in the system [8, 9].

Circular annular fins, one of the most common types of fins, are widely used in many industrial and engineering applications [10-12] from ventilation to heat-recovery systems. Therefore, many experimental or numerical studies have investigated the effect of key geometrical parameters on the heat transfer and pressure drop performance of different finned-tube heat exchanger designs [13-19]. Using extended surfaces boosts the air-side heat transfer. However, their implementation is associated with additional design, material, and manufacturing costs, and the careful optimisation of the fin characteristics is key of helping constrain these costs. For this reason, several studies on fin optimisation are found in the literature with the common goal of reducing the fin volume, thickness and, consequently, weight [20-22].

In fin-optimisation – i.e., weight-reduction – problems, the optimisation parameters may be divided into two main categories, namely, thickness and shape. Fin thickness optimisation itself can be performed with two distinct methods, namely: (i) the continuous-, and (ii) the stepwise-thickness variation methods. The continuous-thickness variation approach aims at obtaining the optimum continuous surface profile of fins. For example, Dhar and Arora [23] used this approach to optimise the fin profile and reduce the fin weight for a fixed required heat dissipation. In the second approach, the fin profile exhibits stepwise-thickness variations; in other words, the fin is built up from a number of individual strips of constant thickness. Kundu and Das [24] used the method of Lagrange multipliers to optimise annular circular fins with a step-change in thickness. Deka and Datta [25] used multi-objective genetic algorithm (MOGA) to optimise the thickness of annular fin tube bundle with one step change. In general, manufacturing a stepwise variable thickness is easier and also less expensive than continuous variable thickness. However, one should note that when one employs variable thickness fins, whether these are stepwise or continuous, a manufacturing cost penalty is paid.

A simple and practical approach for fin optimisation without additional manufacturing cost penalty is to change the annular fin shape. Annular elliptical fins are a good candidate for replacing circular fins. Elliptical-shape fins cause considerably less pressure drop and increase the heat transfer flux in comparison to circular fins [26]. Kundu and Das [27] proposed an approximating method to calculate the annular elliptical fin efficiency, using a series of Bessel functions. Based on a large set of numerical simulations, Nemati and Samivand [28] proposed a correlation to predict the efficiency of all three major types of fins, rectangular, circular and elliptical fins. Later, they used dimensionless parameters to maximise the heat dissipation rate for an annular elliptical fin with a specified fin volume [29].

Beyond the optimisation parameters, the heat transfer boundary conditions affect the accuracy of the optimisation results. In some optimisation studies, a predefined linear, polynomial or exponential temperature distribution over the fin length has been assumed. For example, Duffin and McLain [30, 31] optimised straight fins assuming a linear temperature distribution along

the fin length. Arauzo *et al.* [32] used a ten-term power series to simulate the temperature distribution in an annular fin with hyperbolic profiles. Dhar and Arora [23] assumed exponential temperature distributions over the fin length. Recently, some researchers assumed a constant heat-transfer coefficient across the tube bundle as the heat transfer boundary condition [24, 25, 27, 29].

However, the heat transfer rate does not only change from a tube row to another but also locally over a fin. Therefore, it is not recommended to consider a constant heat transfer coefficient across the tube bundle in optimisation problems, as it results in similar fin geometries for all rows throughout the heat exchanger, which can lead to sub-optimal solutions.

The present study is concerned with the local shape optimisation of multi-row annular finned-tube heat exchangers and focuses on a case study of a four-row heat exchanger design. Unlike in previous researches in this field, the shape optimisation performed in this study involves the consideration of each row independently, without implying constant heat transfer coefficients across the tube bundle. This results in a non-homogeneous bundle, where each row of fins has its own shape, which may be different from that of other rows across the heat exchanger. To present a comprehensive optimisation study and address the most important questions that designers may face in designing such heat exchangers, we investigate four optimisation cases:

1) maximising the heat flux;
2) minimising the pressure drop across the fin rows;
3) minimising the pressure drop and maximising the total heat transfer; or,
4) minimising the entropy generation in the proposed heat exchanger.

This paper is organised as follows. The computational fluid-dynamic (CFD) methods are presented in Section 2, which ends with a model validation subsection, where the heat transfer coefficients and pressure drops predicted by the CFD model are compared to high-fidelity experimental data obtained at different flow regimes. The validated CFD model is then used to conduct a short preliminary study, presented in Section 3, aimed at showing the potential of a local shape optimisation (i.e., resulting in a non-homogenous fin shape throughout the bundle). The local optimisation algorithm together with the four optimisation scenarios are described in Section 4. Response-surface methods are then used to determine the optimal fin-shape repartitions across the bundle corresponding to the four optimisation scenarios mentioned above. These results are presented and discussed in Section 5, and the key conclusions of the present investigation are drawn in the final section (Section 6).

2- CFD Methods

2-1- Problem description

Fig. 1 shows a picture of a typical circular annular finned tube, made of a central tube surrounded by thin circular annular fins. In an air-cooled heat exchanger, several finned-tube rows are placed near to each other, thus creating a tube bundle through which air flows to cool down the working fluid circulating within the tubes. This work aims at enhancing and

locally optimising the fin shape of a baseline tube-bundle configuration (shown in Fig. 2), made of 1-inch (25.4-mm) diameter tubes with 2¼-inch (57.15-mm) diameter fins, placed in a four-row staggered arrangement with a vertical pitch of 2.5 inches (63.5 mm). On a single finned-tube, the 1/64-inch (~0.4-mm) thick fins are evenly spaced, with a fin density of 9 FPI (which denotes fin per inch of tube length), see Fig. 1. This finned-tube geometry is widely used in industrial air-cooled heat exchangers [33, 34].

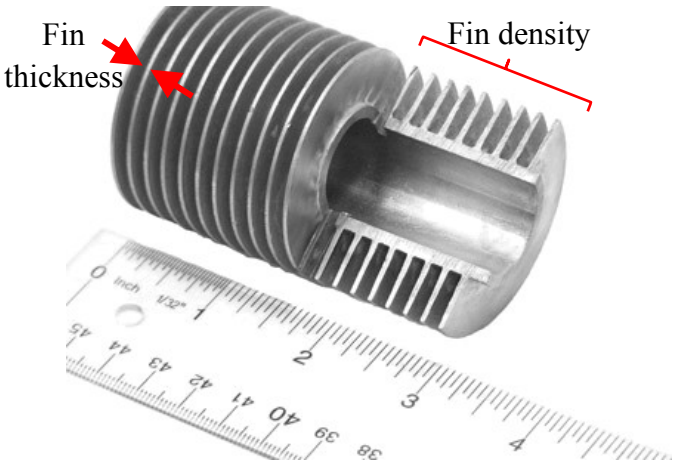

Fig. 1: General view of a circular annular finned tube (Recoloured) [35].

2-2- Computational domain and boundary conditions

A schematic side view of the baseline geometry is shown in Fig. 2a, where the computational domain used to simulate the flow and heat transfer in the finned-tube bundle is highlighted as the area between two dashed-line symmetry surfaces. Due to flow-pattern and geometrical symmetries, this part is a representative unit area. The resolution of the set of governing equations on this area only, using symmetry boundary conditions, allows simulating the flow in the whole bundle while reducing significantly the computational cost and time. The surfaces passing through the middle of fin thickness and fin spacing (see Fig. 2b) are also selected as symmetry surfaces.

In order to avoid inlet and exhaust effects on both heat transfer and pressure drop, the computational domain is extended upstream (by 75 mm) and downstream (by 245 mm) of the tube bundle, as shown in Fig. 2. The turbulent airflow inlet boundary condition imposes uniform and constant velocity (3.5 m/s based on recommendations of Refs. [36, 37]) and temperature (300 K) upstream of the tube bundle, with a 2 % turbulent intensity [26, 38]. All the other thermo-physical properties are considered constant and evaluated at the mean temperature of the domain.

Both tubes and fins are made of aluminum, assuming a constant thermal conductivity. A 400-K uniform and constant Dirichlet condition is imposed on the inner-tube boundaries. Heat is transferred through the fin material by pure conduction and is dissipated towards the flowing air by convection, while radiation is neglected.

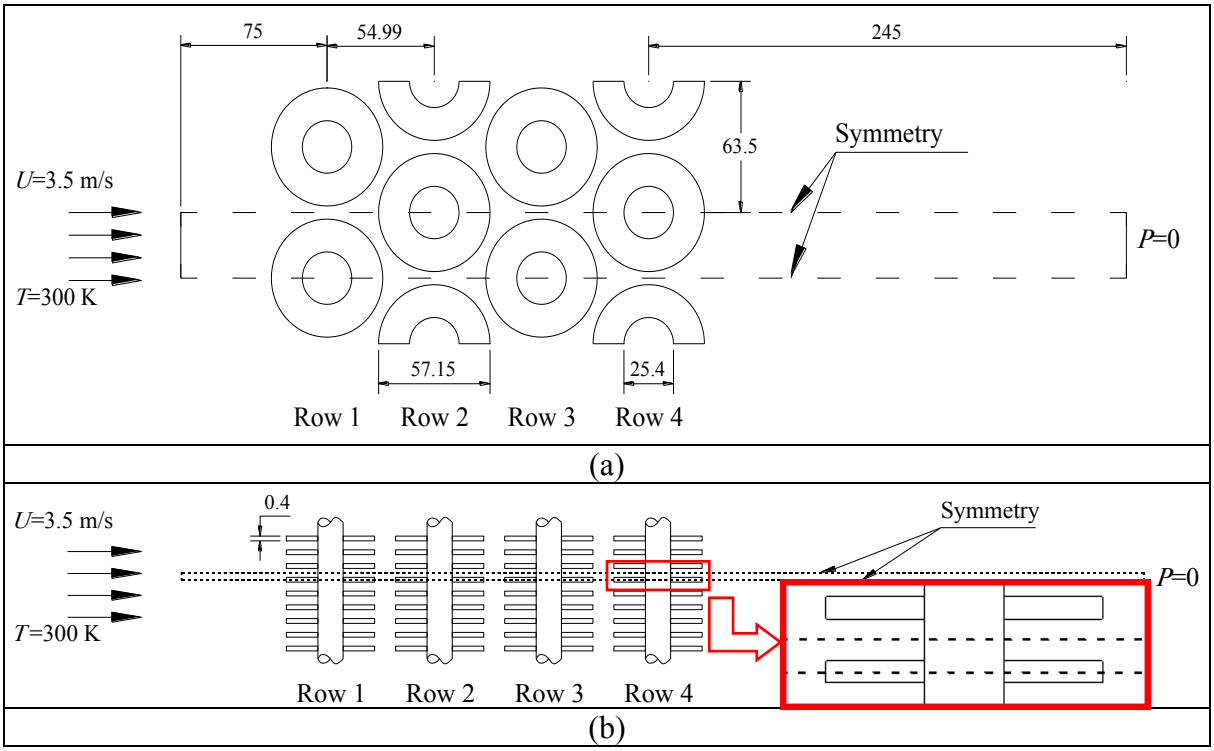

Fig. 2: Schematic layout of the basic geometry in this study: a) side view, b) top view with a zoom-in image of two consecutive fins and computational domain (dimensions are in mm).

2-3- Governing equations and CFD settings

For the incompressible, turbulent air flow in steady-state conditions, the governing equations, i.e., continuity, momentum- and energy-conservation equations, are defined below using index notations, where i and j indices refer to the three spatial dimensions: $(i, j) \in (1,2,3)$.

The continuity equation is expressed as:

$$\frac{\partial}{\partial x_i}(\rho u_i) = 0\,, \tag{1}$$

the momentum-conservation equation reads:

$$\rho\left(u_i \frac{\partial u_j}{\partial x_i}\right) = -\frac{\partial P}{\partial x_i} + \frac{\partial}{\partial x_i}\left(\mu_{\text{eff}} \frac{\partial u_j}{\partial x_i}\right), \tag{2}$$

and the energy-conservation equation is defined in the fluid domain as:

$$\frac{\partial}{\partial x_i}[u_i(\rho e + P)] = \frac{\partial}{\partial x_i}\left(k_{\text{eff}} \frac{\partial T}{\partial x_i}\right), \tag{3}$$

where e is the total specific energy. The terms μ_{eff} $(= \mu + \mu_{\text{t}})$ and k_{eff} $(= k + k_{\text{t}})$ are the effective dynamic viscosity and thermal conductivity, respectively, defined as functions of the turbulent viscosity, μ_{t}, and the turbulent thermal conductivity, k_{t}, both of which are zero in laminar flows.

Finally, the energy-conservation equation in the fin solid domain is written as:

$$\frac{\partial^2 T}{\partial {x_i}^2} = 0\,. \tag{4}$$

The contribution of turbulence is simulated using a transition SST (shear stress transport) model [39]:

$$\frac{\partial}{\partial x_i}(\rho u_i \kappa) = \gamma P_\kappa - \beta_1 \rho \kappa \omega + \frac{\partial}{\partial x_i}\left[\left(\mu + \frac{\mu_{\mathrm{t}}}{\sigma_\kappa}\right)\frac{\partial \kappa}{\partial x_i}\right]; \tag{5}$$

$$\frac{\partial}{\partial x_i}(\rho u_i \omega) = A\rho S^2 - \beta_2 \rho \omega^2 + \frac{\partial}{\partial x_i}\left[\left(\mu + \frac{\mu_{\mathrm{t}}}{\sigma_\omega}\right)\frac{\partial \omega}{\partial x_i}\right] + 2(1-F_1)\rho\frac{1}{\omega\sigma_{\omega,2}}\frac{\partial \omega}{\partial x_i}\frac{\partial \kappa}{\partial x_i}. \tag{6}$$

S is the strain rate magnitude and A is constant. Eqs. (5) and (6) involve two additional variables that are the turbulent kinetic energy, κ, and the specific turbulence dissipation rate, ω, from which one can evaluate the value of the turbulent viscosity, μ_t, as:

$$\mu_{\mathrm{t}} = \frac{\alpha\rho\kappa}{\max(\alpha\omega, SF_2)}. \tag{7}$$

and F_1 and F_2 are blending functions in SST mode which limit the eddy viscosity in the boundary layer region. Eqs. (8) and (9) are used to determine the damping function, γ, and the parameter Π, which shows the local stability of the flow in the near-wall region:

$$\frac{\partial}{\partial x_i}(\rho u_i \gamma) = \left(P_{\gamma,1} + P_{\gamma,2}\right) - \left(E_{\gamma,1} + E_{\gamma,2}\right) + \frac{\partial}{\partial x_i}\left[\left(\mu + \frac{\mu_{\mathrm{t}}}{\sigma_\gamma}\right)\frac{\partial \gamma}{\partial x_i}\right]; \tag{8}$$

$$\frac{\partial}{\partial x_i}(\rho u_i \Pi) = P_{\Pi,t} + \frac{\partial}{\partial x_i}\left[\sigma_{\Pi,t}\left(\mu + \frac{\mu_{\mathrm{t}}}{\sigma_\gamma}\right)\frac{\partial \Pi}{\partial x_i}\right]. \tag{9}$$

In Eq. (8) and Eq. (9) $P_{\gamma,1}$ and $P_{\gamma,2}$ are production terms and $P_{\gamma,2}$ and $E_{\gamma,2}$ are destruction terms which are determined by:

$$P_{\gamma,1} = 2F_{\mathrm{length}}\,\rho S(\gamma F_{\mathrm{onset}})^{c_{\gamma 3}}$$
$$P_{\gamma,2} = 2c_{\gamma 1}\rho\Omega\gamma F_{\mathrm{turb}} \tag{10}$$

and,

$$E_{\gamma,1} = \gamma P_{\gamma,1}$$
$$E_{\gamma,2} = c_{\gamma 2}\gamma P_{\gamma,2} \tag{11}$$

F_{length} is responsible for controlling the length of the transition zone and is an empirical function correlation, and Ω is the vorticity magnitude. $c_{\gamma 1}$, $c_{\gamma 2}$, and $c_{\gamma 3}$ are constants. The transition onset is also controlled by the F_{onset}. Interested readers can refer to Ref. [40] for more detailed discussions about this method. The capability of this method to simulate both laminar and turbulent regimes has been approved previously [41, 42].

For the basic geometry shown in Fig. 2, the region in the fin spacing is discretized with structured elements, while unstructured elements were employed for the other areas. A grid

dependence study was performed (involving $>10^6$ nodes), to ensure that results were independent of grid density (Table 1). Moreover, grids were adapted to keep, y^+, defined in Eq. (12), at a value below 3:

$$y^+ = \frac{\rho \Delta y \sqrt{\tau_w/\rho}}{\mu}, \tag{12}$$

where τ_w is the wall shear stress and Δy the distance from the first grid node in the fluid domain to the nearest wall surface. Fig. 3 shows a zoom-in section of the generated grid.

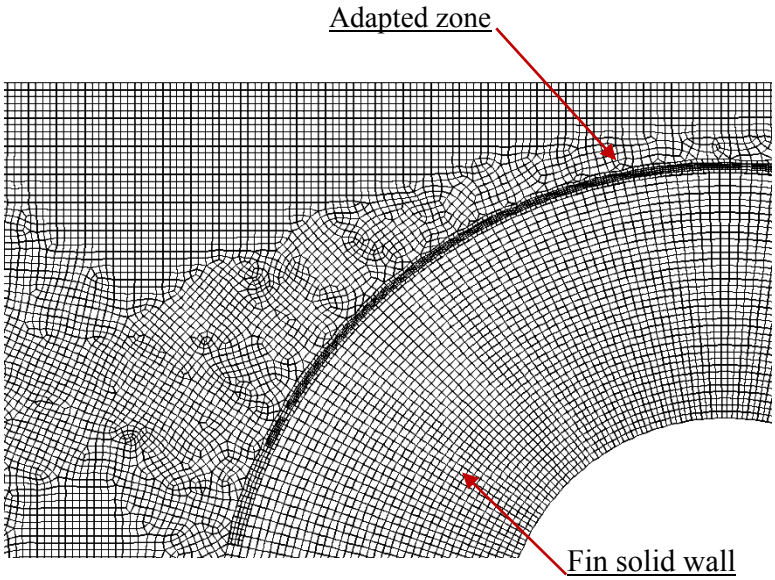

Fig. 3. A zoom-in section of the generated grid.

Table 1: Grid independence study results.

Number of nodes	Average pressure drop (Pa)	Average outlet temperature (K)	Maximum Relative Error
1.04E+06	85.21	373.5	---
8.84E+05	85.03	373.5	0.21%
3.84E+05	84.85	371.9	0.42%
1.17E+05	82.86	372.3	2.76%

The steady-state turbulent fluid flow in the domain was solved using the Fluent solver module, ANSYS 19.1. A SIMPLE (semi-implicit method for pressure-linked equations) scheme was selected for solving the pressure-velocity coupling, while a second-order method was selected to discretize pressure and energy equations. The momentum conservation equation was finally discretized using a second-order upwind method. Other equations (Eqs. (8) and (9)) were also discretized by first-order methods. Maximum acceptable residuals for velocities and continuity equations were set to 10^{-5} and to 10^{-6} for the energy

conservation equation. The residuals were set to 10^{-4} for the other equations. Moreover, mass-weighted averages of the pressure drop, as well as outlet temperature, were monitored in every iteration, to ensure the simulation convergence. Eventually, the global heat transfer coefficient and pressure drop were calculated as the main outputs of the simulation.

2-4- CFD model validation

Two dimensionless parameters, the Nusselt and Euler numbers, are computed to validate the computational methods used to simulate the turbulent flow in the tube bundle. The numerical results are verified against experimental correlations from Ref. [43], for both Nu and Eu:

$$Nu = \frac{h d_{\mathrm{ot}}}{k}, \tag{13}$$

$$Eu = \frac{\Delta P}{\rho u_{\max}{}^2}, \tag{14}$$

where ρ and k are the air density and thermal conductivity, respectively, and d_{ot} is the outer-tube diameter. The method of extracting the overall heat transfer coefficient, h, from numerical results is discussed in detail in Ref. [26]. The comparison of numerical simulation and experimental results [43] for both Nu and Eu are presented in Fig. 4 and 5, respectively. The figures show a good agreement between the numerical and experimental results. Reynolds number in Fig. 4 and 5 is defined as:

$$Re = \frac{\rho u_{\max} d_{\mathrm{ot}}}{\mu}, \tag{15}$$

in which μ is the dynamic viscosity. $u_{\max}$ is the maximum uniform flow velocity inside the bundle [43], defined as:

$$u_{\max} = \frac{U s_t s_f}{(s_t - d_f) s_f + (d_f - d_{ot})(s_f - \delta)}, \tag{16}$$

In the above equation, U is the inlet velocity, s_t and s_f are the tube transverse pitch and fin pitch, respectively. δ is the fin thickness. In Fig. (5) and Fig. (6), Err. is defined as:

$$\mathrm{Err.} = \frac{|\text{Numerical value} - \text{Reference value}|}{\text{Reference value}} \times 100, \tag{17}$$

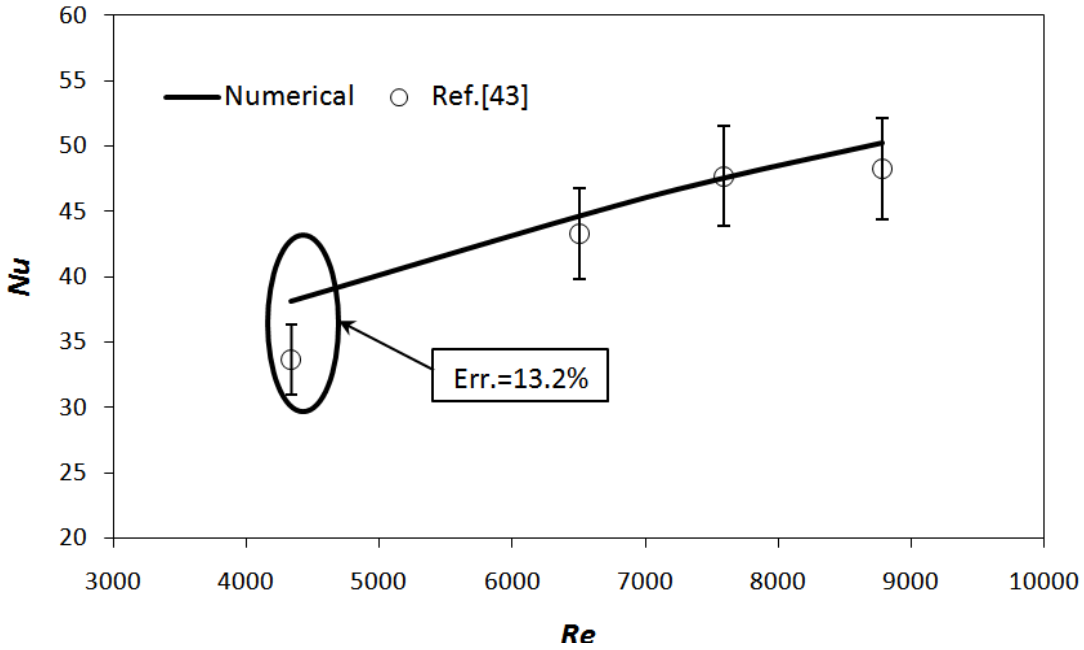

Fig. 4. Comparison of the mean Nusselt number, Nu, obtained from numerical simulation and experimental correlation [43] (Experimental error bar: ±8 %), as a function of the mean Reynolds number in the tube bundle.

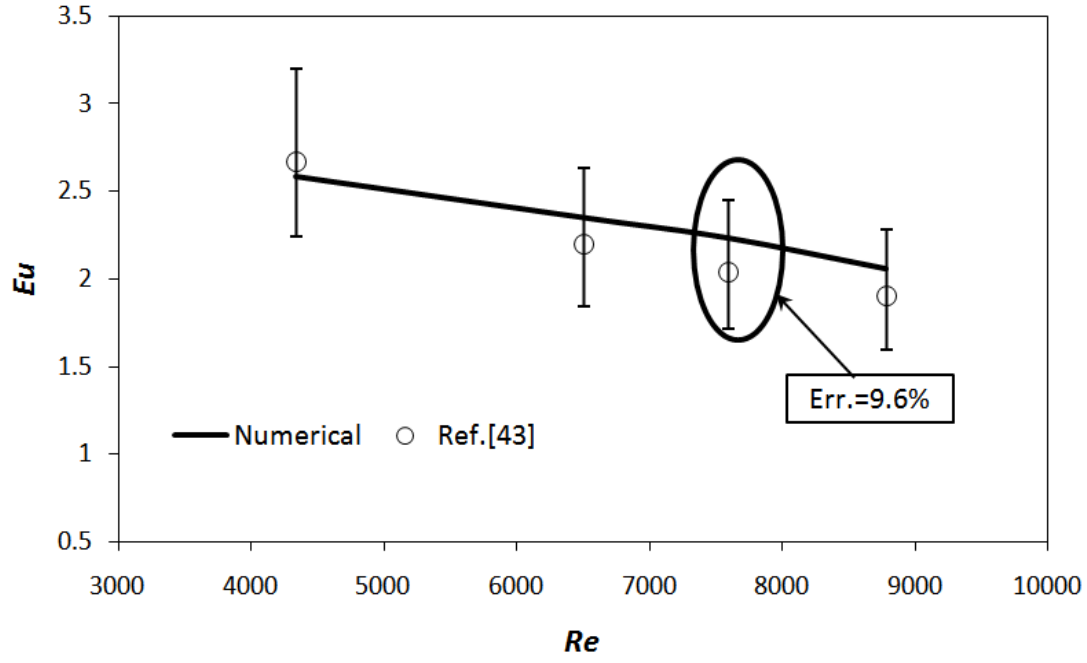

Fig. 5. Comparison of the mean Euler number, Eu, obtained from numerical simulation and experimental correlation [43] (Experimental error bar: -16 %, +20 %), as a function of the mean Reynolds number in the tube bundle.

3- Preliminary Study: Potential of Local Optimisation

Before running the optimisation, a preliminary study is conducted to investigate the proposed idea in this study, i.e., the possibility of independent fin optimisation in each row. In this investigation, the effects of the individual row on the thermo-fluidic behavior of the unit are studied to justify the necessity of running independent shape optimisation for each row.

As the initial step of the preliminary study, at first, it is investigated why elliptical fin shape is justifiable from an engineering perspective. To answer that, the effects of a circular finned tube bundle on the thermal performance of the unit is investigated. The flow temperature contour of a circular finned tube bundle is shown in Fig. 6. As displayed, the contribution of fin area in heat transfer across the unit is not uniform (Please see the non-uniform circumferential temperature distribution in fins across the unit). A high-temperature zone (dark orange region in Fig. 6) is formed at the back of the fins (the side which locates in a further distance from the inlet) and this high-temperature zone grows from the outermost left fin (the first fin which is the closest one to inlet) to the outermost right one/the 4th one (please see Fig. 6-b and 6-c). In addition, as displayed in Fig. 6-d, there is a dead zone behind the circular fin due to flow separation over the fin edge. The flow circulation behind the fin prevents the flow in this zone to be mixed with the adjacent zone. Therefore, a considerable temperature rise is observed behind the fin, which means that less heat transfer takes place. Interested readers can refer to Refs. [26, 38] for more detailed discussions about flow patterns around annular fins. Owing to these facts, it is expected that the fin area can be partly reduced without any considerable impact on the overall heat transfer. The necessity of this reduction gets clearer if one knows that for a 1-m finned tube with 2.11-mm tube thickness, the weight of a 1-m bare tube is 458 g, while the weight of the fin itself is 790 g.

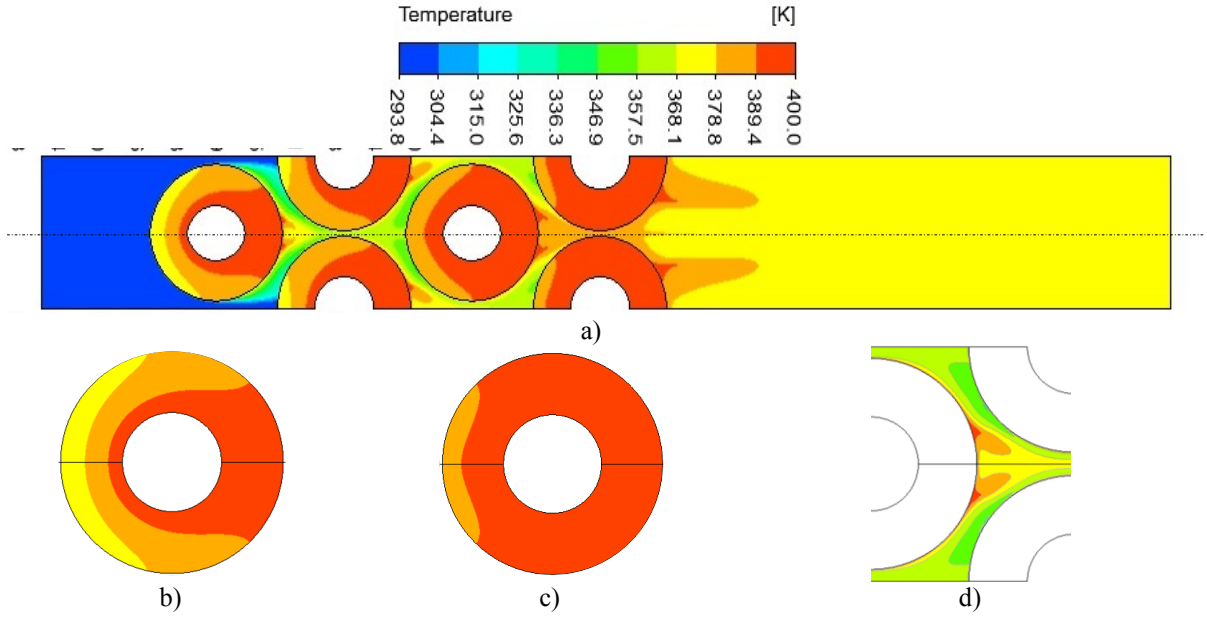

Fig. 6. Flow temperature contour of the circular fin at the symmetry plane passing through the fins: a) over the entire tube bundle; b) focused on the 1st fin in full display, c) focused on the 4th fin in full display, d) focused on the airflow temperature distribution downstream of the 2nd fin.

The second step of this preliminary study is a comparison of the thermo-fluidic behaviors of the unit for 5 different cases. The results of these comparisons are shown in Fig. 7 and 8, respectively for the velocity and temperature fields. The first configuration presents the baseline case, i.e., where all the fins across the tube bundle are circular. In the next four configurations, all fins are elliptical, except those located at a specific row. The location of the circular fins in the tube bundle is varied from the first to the fourth and last row, to

observe its impact on both the overall drag and heat transfer. In these studies, the geometry of the elliptical fins is based on that of the circular fins, with a minor diameter of 46.75 mm (instead of 57.15 mm in the circular shape) on the vertical axis. The annotations of 1st to 4th rows respectively refer to the outermost left and counts on to the outermost right fin.

As observed in Fig. 7, when the 4th fin row is circular, the circulation zone generated behind the fin is much longer, in comparison with the others. On the other hand, regardless of the tube row location, the average (i.e., bulk) velocity in front of a circular fin is higher than in front of an elliptical one due to passage blockage, which consequently causes more pressure drop on that row. In addition, although the flow passing the circular fin gets warmer in comparison with elliptical fins due to more heat transfer area, the average fin temperature in the elliptical fin is higher.

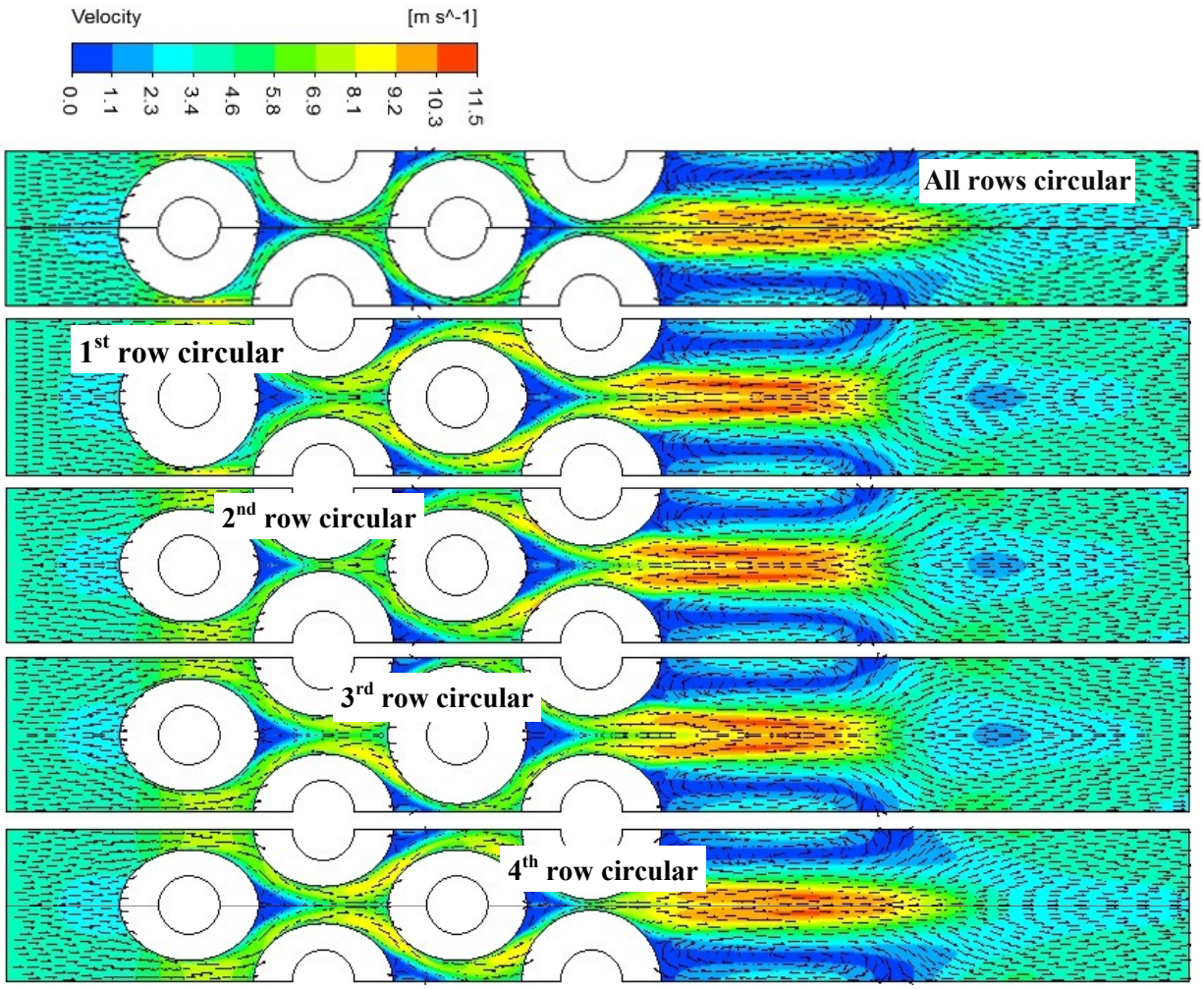

Fig. 7. Comparison of the velocity fields in different geometries

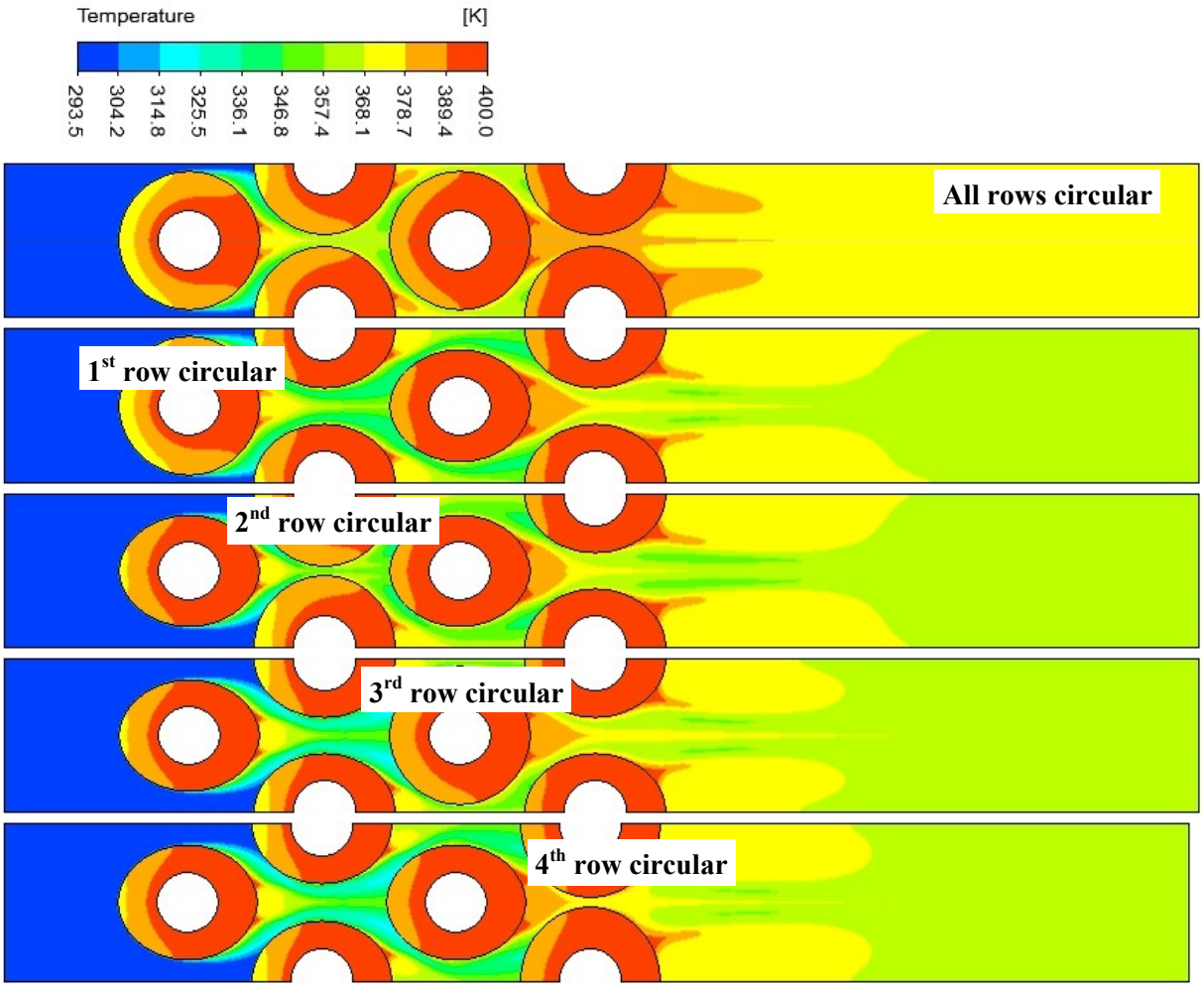

Fig. 8. Comparison of the temperature contours in different geometries.

The summary of all the above evidence shows that fins must approach the elliptical shape to reduce the pressure drop. Furthermore, as shown in Fig. 8, the first row exhibits the highest heat transfer rate, because the first row is directly in contact with the fresh unheated air, unlike the rows downstream. Thus, a circular first-row fin – which is the shape with the highest heat transfer area – is preferred to achieve high heat transfer rate. These results justify the proposed local optimisation study presented in the next section.

To further investigate the impact of varying locally a single-fin diameter, a parametric study was performed, whereby a single row minor-axis diameter is varied, while all remaining fins are circular. Fig. 9 shows the influence of this local variation on the mean heat flux and overall pressure drop. First, it is observed that varying the fin diameter of different rows does not have a similar impact on the overall performance of the bundle heat exchanger. In particular, the overall heat flux appears to depend strongly on the fin diameter of the second row, while the shapes of the other rows have less significant impact. These discrepancies support the approach chosen in this study that is to perform a local fin-shape optimisation.

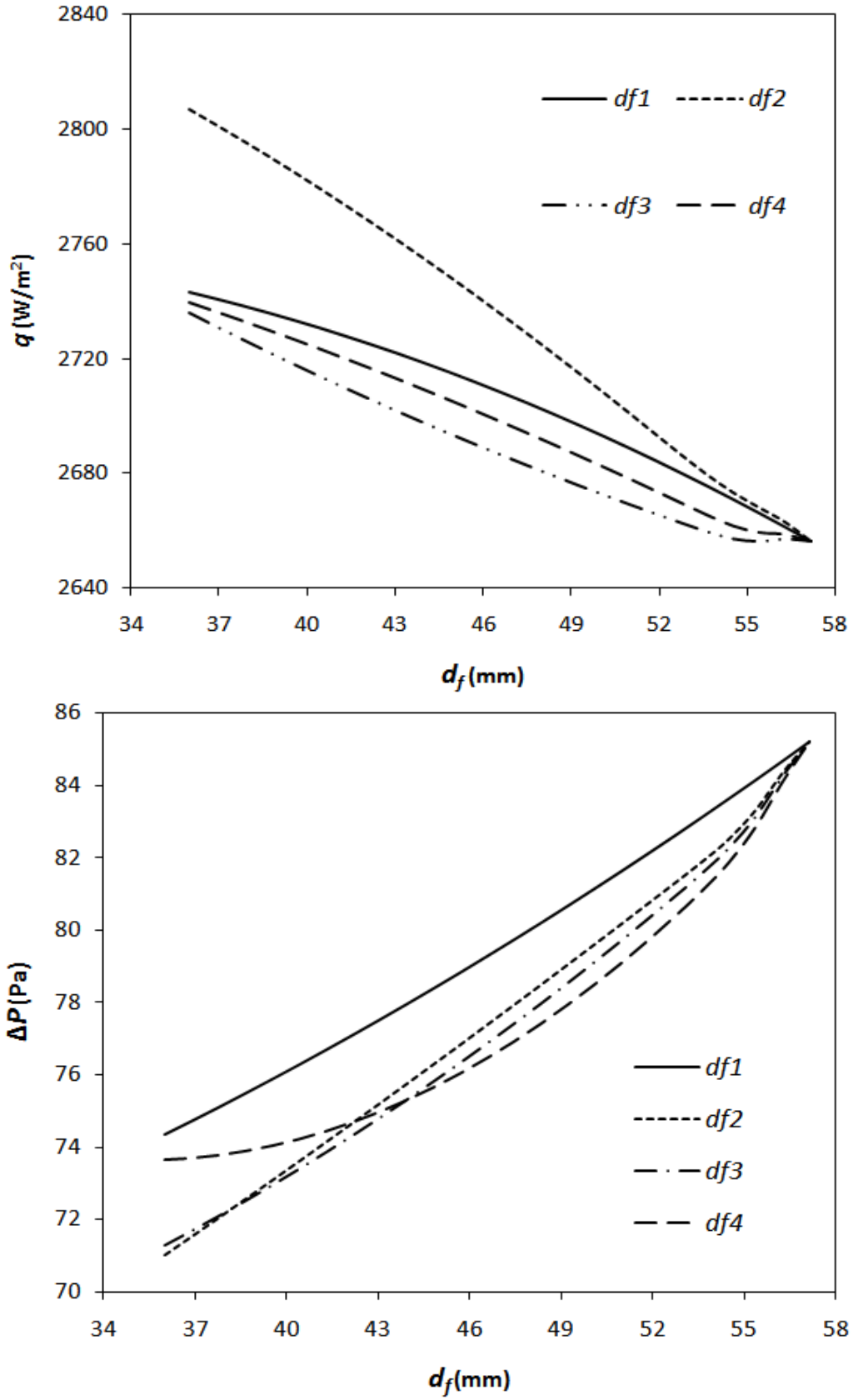

Fig. 9. Variations of heat flux and pressure drop with respect to each vertical fin diameter.

4- Optimisation Methods

4-1- Optimisation scenarios

The set of decision variables used in the following optimisation studies is made of the four vertical diameters of each individual fin row, referred to as the minor diameters (vertical diameters) $\bar{d}_{f1}$ to $\bar{d}_{f4}$. Inequality constraints are added on each of these geometrical dimensions that are allowed to vary in a range contained between 36.0 mm and 57.15 mm (please see Fig. 10). Other geometrical parameters (including the horizontal and vertical tube pitches, the horizontal major axis diameter, the bare tube outer diameter, and the entrance and exit lengths of the computational domains) are defined constant throughout the optimisation process and defined according to the dimensions presented in Fig. 1.

Four practical optimisation scenarios (i.e., objective functions) are defined below to present a comprehensive optimisation study and fulfill various designers' needs:

Case 1) Design the lighter heat exchanger by minimising the fin area and maximising heat transfer rate in the heat exchanger or simply by maximizing the heat transfer rate per unit area (heat flux).

Case 2) Design an exchanger (e.g., air cooler) with minimum fan power consumption by minimising the pressure drop across the fin rows of the exchanger.

Case 3) Design an exchanger with reasonable fan power consumption and efficient overall heat transfer by minimising the pressure drop and maximising the total heat transfer rate in the heat exchanger.

Case 4) Design an exchanger based on minimum entropy generation, to justify the fan power used to compensate the airside pressure drop for heat removing.

In essence, the optimisation formulation finds the best local configuration of vertical fin diameters to satisfy the objectives determined for each case.

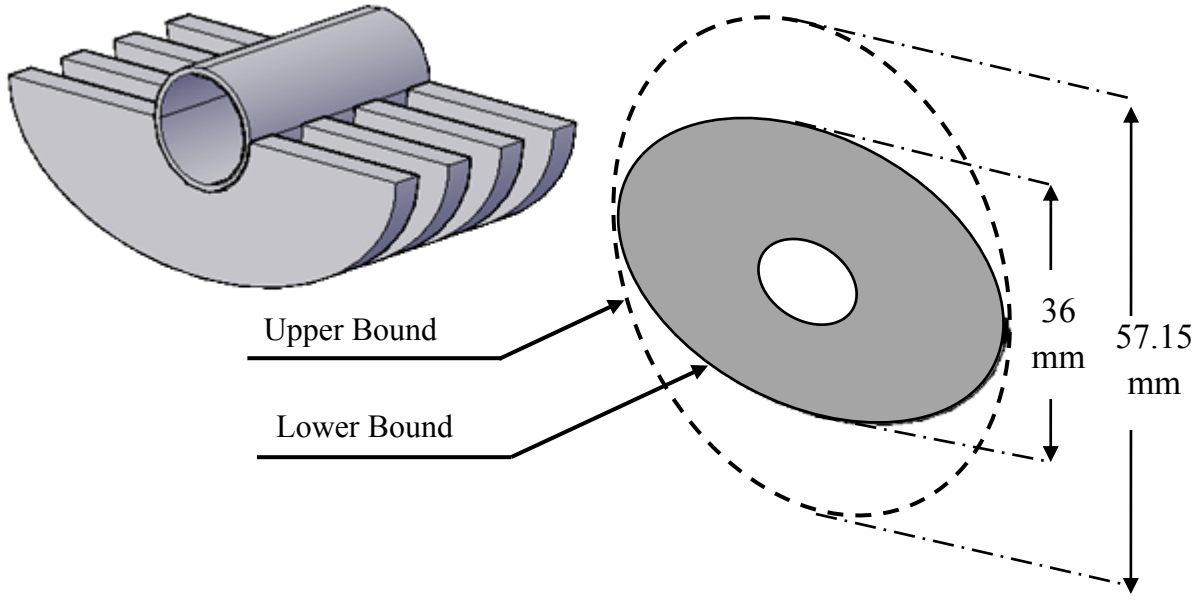

Fig. 10: Constraint imposed on each finned tube row.

4-2- Optimisation methods

In the general form, multi-objective optimisation can be presented as [44]:

Minimise/ maximise:

$$f_{\mathrm{m}}(x), \quad m = 1,2,\dots M;$$

Subject to:

$$\begin{aligned} g_{\mathrm{j}}(x) \geq 0, \quad \mathrm{j} = 1,2,\dots J; \\ h_{\mathrm{k}}(x) = 0, \quad \mathrm{k} = 1,2,\dots K; \\ x_i^{(L)} \leq x_i \leq x_i^{(U)}, \quad i = 1,2,\dots I, \end{aligned} \tag{18}$$

In which $f_{\mathrm{m}}(x)$ is the optimisation objective function and M is the total number of functions to be optimised. x is a solution vector of n decision variables i.e. $x = (x_1, x_2, \dots, x_n,)^T$. The constraint functions of this problem are $g_{\mathrm{j}}(x)$ and $h_{\mathrm{k}}(x)$, where j and k are the numbers of inequality and equality constraints, respectively. The last set represents the variable bounds within the specified lower limit $x_i^{(L)}$ and $x_i^{(U)}$. The goal of multi-objective optimisation is to obtain a set of solutions that are not dominated by other solutions [44]. A solution x_1 is to dominate solution x_2 if the two following conditions are verified [44]:

- The solution x_1 is no worse than x_2 in all objectives;
- The solution x_1 is strictly better than x_2 in at least one objective.

These non-dominated solutions are often called Pareto optimal solutions. It is not possible to determine which one of the non-dominated solutions is better than the other. However, the solutions in the non-dominated set are better than those in the remaining design space [44].
For the optimisation studies, ANSYS DX (DesignXplorer) was used. This optimisation tool is a response-surface based module. To construct the response surfaces, at first, the design of experiments (DOE) was performed to generate design points. In this study, 27 auto-defined central composite designs were specified for 4 defined decision variables, i.e., the vertical fin diameters of each row. The thermo-fluid problem was solved for each of those sampling design points and the values of the four objective functions (as defined in section 4.1) extracted. The kriging method [45] was employed to generate the response surface for the output parameters. This method is a meta-modeling algorithm with an improved response quality, which fits higher-order variations of the output parameters. The determination of the optimum location of those surfaces was performed by using either the MOGA (multi-objective genetic algorithm) approach or a screening followed by the NLPQL (nonlinear programming by quadratic Lagrangian) method. The former (MOGA) was used for multi-objective optimisation cases (case 3 in section 4.1), while the latter (screening approach followed by the NLPQL method) was used for the single-objective optimisation cases (case 1, 2 and 4 in section 4.1). For more information on the design point generations, response-surface constructions, and the optimisation approaches, please refer also to the literature [46-50].

Selecting the best solution among the points on Pareto front is not simple and straightforward. For multi-objective optimisation, the sample set on each Pareto surface is sorted by a decision support process to extract the best candidates. In this study, the decision-making technique available in Ansys software was used. This method is a goal-based, weighted, aggregation-based design ranking technique [51], which was used to find the best candidate point. In this method, the design candidates are ranked based on the single weighted objective function. This weighted objective function is specified by the user, based

on the importance of the performance parameters and decision variables. In this study, all the design parameters and decision variables were assumed to have equal importance. Therefore, default values were used [51].

5- Optimisation Results

To generalise the results of the study, the scaled form of input variables as well as goal parameters are implemented. The introduced parameters are normalised by dividing them by their corresponding values in the circular case, which are reported in Table 2. In this table, the subscript "c" refers to the baseline circular case.

Table 2: The scaled form of variables.

Symbol	Description
$\bar{d}_{\mathrm{f}i} = \frac{d_{\mathrm{f}i}}{d_{\mathrm{fc}}}$	Scaled fin vertical diameter of ith row
$\bar{q} = \frac{q}{q_{\mathrm{c}}}$	Scaled heat flux
$\bar{Q} = \frac{Q}{Q_{\mathrm{c}}}$	Scaled total heat transfer
$\bar{S_{\mathrm{g}}} = \frac{S_{\mathrm{g}}}{S_{\mathrm{g,c}}}$	Scaled total entropy generation
$\Theta = \frac{T_{\mathrm{out}} - T_{\mathrm{w}}}{T_{\mathrm{in}} - T_{\mathrm{w}}}$	Scaled approach temperature
$\overline{\Delta P} = \frac{\Delta P}{\Delta P_{\mathrm{c}}}$	Scaled pressure drop
$\bar{W} = \frac{W}{W_{\mathrm{c}}}$	Scaled fin weight

The scaled approach temperature definition is also presented in Table 2. This factor presents the closeness of the airside outlet temperature to its maximum value, i.e., the tube wall temperature. The limit of this factor to one and zero leads to no heat transfer case and maximum possible heat transfer, respectively.

5-1- Case 1: Maximising heat flux

Minimising the fin area is the key to designing cost-effective heat exchangers, as extended surface areas are associated with material and manufacturing costs. However, this minimisation should not penalise the thermal performance of the unit. A single-objective optimisation problem is thus solved in this section, whereby the overall average heat flux (defined as the overall heat transfer rate per unit of total heat transfer area) is maximised.

It's noteworthy that since this optimization study is a single objective optimization problem, therefore, the optimization solution reaches on single utopian solution. The suggested optimum point for this optimisation is tabulated in Table 3. Based on the results, to maximise the total heat transfer rate and minimise the fin area, the 1st row must be kept circular, while other rows should be changed to a horizontal ellipse with minimum vertical diameter. Indeed, by comparison of optimum case with the base case (all fins circular), one concludes that fin weight can be reduced 35% for a 22% penalty on total heat transfer rate. Such a trend can be attributed to the fact that the optimum point keeps the geometry of the first row circular, as the dominant geometrical parameter in heat transfer (as shown in preliminary studies), to maximise heat transfer rate and changes the shapes of the 2nd to 4th row to minimum possible ellipse, significantly reducing the material cost of the unit (see Fig. 11).

The suggested changes in the fin geometry can be interpreted as follow: Since the first row is faced with the unheated fresh air and has the most local temperature difference among the other rows (as shown in Fig. 8, therefore, it is reasonable to keep the heat transfer area of this row as large as possible. This means that the circular shape of fin in the first row should be kept intact. For the other rows, the fin sides of each row are located in the heated stream of a previous row and consequently, the local temperature difference is relatively small. Therefore, there is no reason to keep these areas large anymore and the shapes of fins in those rows are changed to an oval shape. These shape changes increase the passage area between consecutive fins where the fluid will be less affected by the fin presence and consequently make the fin frontal areas of these rows be in contact with the colder stream (see Fig. 11). This secondary effect boosts the heat flux at those rows.

Table 3: Geometry optimisation for heat flux.

Name	$\bar{d}_{f1}$	$\bar{d}_{f2}$	$\bar{d}_{f3}$	$\bar{d}_{f4}$	$\bar{q}$	$\bar{Q}$	$\bar{S}_g$	Θ	$\overline{\Delta P}$	$\bar{W}$
Optimum point	1.00	0.63	0.63	0.63	1.15	0.78	0.89	0.43	0.64	0.65

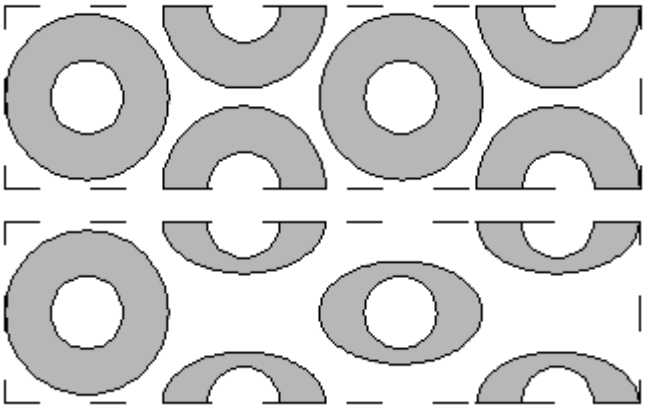

Original geometry (base case)

1st suggested candidate for maximum heat transfer rate per unit area

Fig. 11. Visual comparison of the base case with the optimum candidate (1st suggested candidate) of the 1st case of optimisation scenarios.

5-2- Minimising the pressure drop

The overall pressure drop shall be compensated by fan work and consequently, electricity consumption. Although such parameters are not a serious concern for the designers, in particular for large-scale applications, power consumption can still be a restricting parameter in the design of a heat exchanger unit. For this reason, a local fin-shape optimisation was performed to minimise the pressure drop at a constant air mass flow rate. The result of this optimisation study is listed in Table 4. In addition, the geometry of the optimum candidate along with the base case was displayed in Fig. 12. By comparison of the optimum case with the base case (all fins circular), one concludes that fin weight can be reduced 46% with 50% favorable reduction in pressure drop. As explained previously, and also approved in a previous study by the authors [26], since the maximum velocity in a finned-tube bundle with elliptical fins is less than that in a similar bundle with circular fins, the pressure drop is proportionally smaller. Therefore, it makes sense that all fin rows tend to an elliptical shape with the lowest vertical diameter (lower bound of the optimisation). This result of the optimisation process, confirms the reliability of the conducted optimisation process, which, without any external interference, predicted rational results for the problem.

Table 4: Geometry optimisation for pressure drop.

Name	$\bar{d}_{f1}$	$\bar{d}_{f2}$	$\bar{d}_{f3}$	$\bar{d}_{f4}$	$\bar{q}$	$\bar{Q}$	$\bar{S}_g$	Θ	$\overline{\Delta P}$	$\bar{W}$
Optimum point	0.63	0.63	0.63	0.63	1.11	0.63	0.78	0.54	0.50	0.54

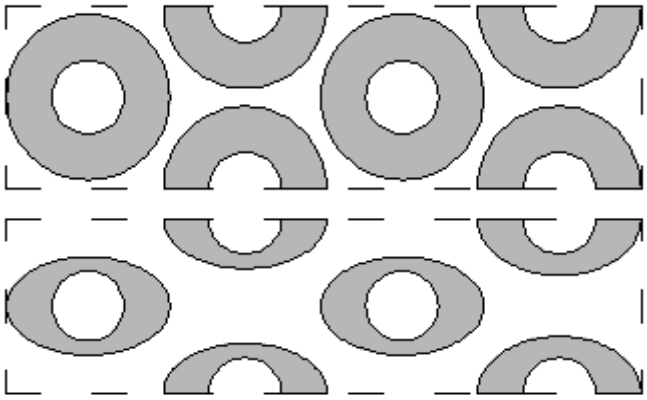

Fig. 12. Visual comparison of the base case with the optimum candidate (2nd suggested candidate) of the 2nd case of optimisation scenarios.

5-3- Minimising the pressure drop and maximising the total heat transfer

One of the most popular optimisation scenarios is defined based on minimising the pressure drop and maximising the total heat transfer rate in the unit. This study is usually designed to minimise the fan power of the system, while the thermal performance of the unit is maximised. Fig. 13 shows the utopian points on the Pareto front. In this Figure, the horizontal axis is the scaled heat transfer rate and the vertical axis is the scaled fin weight. The point with coordinates $[\bar{Q} = 1, \overline{\Delta P} = 1]$ (not shown in the figure) represents a bundle where all fins

are circular. The candidate point is also presented by a star in this Figure. Based on Fig. 13, the pressure drop can be reduced to 0.50 of its original value by the penalty of a 36 % reduction in total heat exchange rate ($\bar{Q}$ = 0.64).

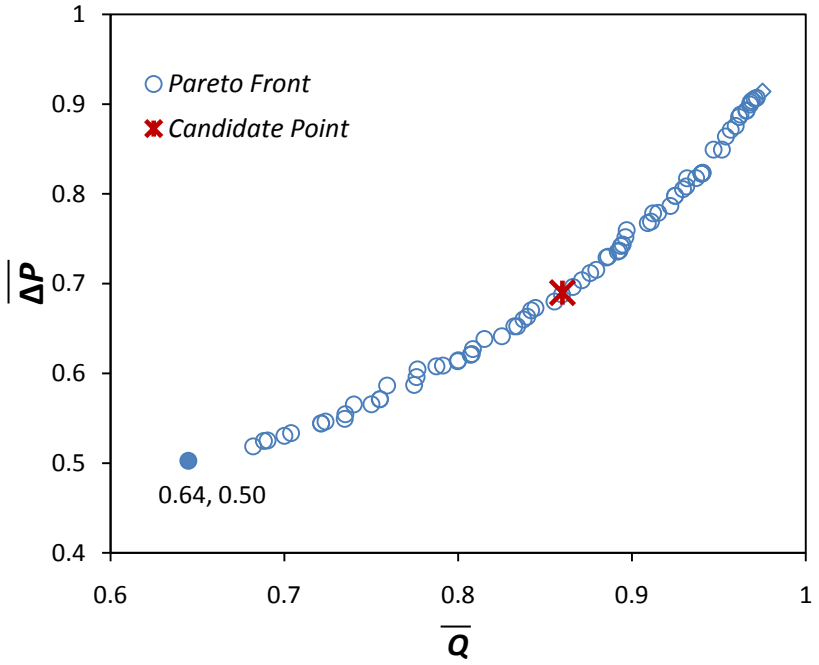

Fig. 13. Pareto front and Candidate point for Case 3.

The candidate point for this optimisation study is tabulated in Table 5. As listed in the table, the 1st row is almost circular, while the other rows are elliptical. However, the trend shape configuration in this table almost starts from the most elliptical fin in the 2nd row to the more circular shape in the last row. Besides, the geometry of this candidate is graphically compared with the base case in Fig. 14. In this case, the total heat transfer, drops by about 14 % in comparison with the baseline case, while the overall pressure drop is reduced by more than 30 % and the material weight by 23 %. Since the optimisation aims at maximizing the total heat transfer rate, it seems reasonable that the first-row shape is kept almost circular. For further discussions, please consult Section 5-1. However, as the pressure drop across an elliptical fin is less than a circular fin [26], elliptical shape is preferred for all other rows (all rows but the first one).

Table 5: Geometry optimisation for total heat transfer rate and pressure drop.

Name	$\bar{d}_{f1}$	$\bar{d}_{f2}$	$\bar{d}_{f3}$	$\bar{d}_{f4}$	$\bar{q}$	$\bar{Q}$	$\bar{S}_g$	Θ	$\overline{\Delta P}$	$\bar{W}$
Candidate Point	0.987	0.640	0.721	0.920	1.09	0.86	0.94	0.37	0.69	0.77

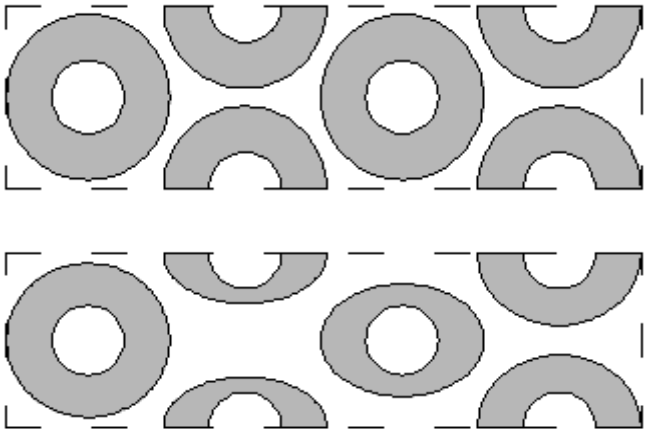

Base geometry

1st suggested candidate for maximising heat transfer and minimising the pressure drop

Fig. 14. Visual comparison of the base case with the optimum candidate (1st suggested candidate) of the 3rd case of optimisation scenarios.

5-4- Minimising the entropy generation

In the previous part, the overall heat transfer and pressure drop have been considered with the same priority in the multi-objective optimisation problem. In this study, entropy is chosen as an index of equivalency of heat transfer and pressure drop. Assuming air as an ideal gas with constant properties, the entropy generation rate can be expressed as:

$$S_{\text{gen}} = \Delta S - \frac{Q}{T_{\text{w}}} \tag{19}$$

where ΔS is defined as:

$$\Delta S = \dot{m}\left[c_{\text{p}} \ln\frac{T_{\text{out}}}{T_{\text{in}}} - R \ln\left(1 - \frac{\Delta P}{P_{\text{in}}}\right)\right] \tag{20}$$

Under this condition, the optimised geometry is listed in Table 6. As listed in the table, the entropy generation rate is minimised if the diameter ratio (minor diameter to major diameter) of all rows is minimised and generates about 22 % less entropy in comparison with the base case. Such geometry is graphically displayed in Fig. 12. The exact similarity observed between the results presented in Table 6 and those presented in Table 4 (i.e., with the pressure drop minimisation scenario) means that the entropy generation in air-side flow through the tube bundle is mainly due to the pressure losses.

Table 6: Geometry optimisation for entropy generation.

Name	$\bar{d}_{f1}$	$\bar{d}_{f2}$	$\bar{d}_{f3}$	$\bar{d}_{f4}$	$\bar{q}$	$\bar{Q}$	$\bar{S}_g$	Θ	$\overline{\Delta P}$	$\bar{W}$
Optimum point	0.63	0.63	0.63	0.63	1.11	0.63	0.78	0.54	0.50	0.54

6- Conclusions

Extended surfaces are applied in heat exchangers used in many industries, including in the heating, ventilation and air-conditioning industry. Using optimised fin shapes is a promising solution for improving thermal performance while minimising additional costs. In this study, a four-row finned-tube heat exchanger is optimised by varying locally the shape of the annular fins, thus resulting in non-uniform tube bundles, although the overall approach is directly applicable to any multi-row heat exchanger design. For each individual fin row, the outer-tube elliptical shape is allowed to vary from a 57.15-mm diameter circular shape (referred to as the baseline shape) to an elongated elliptical shape (where the vertical minor diameter is reduced down to 36 mm, which represents 63 % of the major diameter).

The four vertical diameters applied to each single fin row form the set of decision variables used in the optimisation problem. Four distinct objective functions, corresponding to four practical design strategies and various designers' needs, are used to determine the local fin-shape repartitions throughout the bundle that: (i) maximise the heat flux, (ii) minimise the overall pressure drop, (iii) minimise the pressure drop while maximising the total heat transfer rate, or (iv) minimise the entropy generation.

The first optimisation scenario resulted in a significant decrease of the total fin weight, by 35 % relative to the baseline case in which all the fin surfaces across the tube bundle were circular, while the total heat transfer rate to the flowing air was reduced by only 22 %. The corresponding tube-bundle configuration was a limiting case, where the fins of the flow-entrance row were perfectly circular, while the remaining fins were elongated elliptical fins with the minimum minor diameter (i.e., 36 mm). From the results, it appeared that the turbulence created by the first circular-shaped fins upstream in the heat exchanger favoured the overall heat transfer, while the lightened elliptical fins help reduce the total weight.

The configurations obtained when minimising the overall pressure drop or entropy generation (i.e., corresponding to the second and fourth scenarios) are similar, meaning that the contribution of the pressure losses through the tube bundle to the overall exergy destruction are predominant. As expected, a uniform bundle formed of elliptical-shaped fins with minimum vertical diameters minimises the overall pressure drop, generating 22 % less entropy and reducing the pressure losses by 50 %. However, with this arrangement, the overall heat transfer was reduced by 37 %.

Finally, the results provided by the third optimisation scenario, which aims at reducing the overall pressure drop while maximising the total heat transfer rate, are particularly interesting. The total heat transfer rate, drops by only 14 % in comparison with the baseline

case, while the overall pressure drop is reduced by more than 30 % and the material weight by 23 %. The fin arrangement designed to achieve such a performance is not straightforward, with the entrance and exiting rows made of nearly-circular fins, while inner-bundle rows are made of elliptical-shaped fins. The non-homogeneity of this configuration, together with encouraging results, confirms that the local fin-shape optimisation approach proposed in this work is a promising technique to further increase the performance of finned-tube exchangers while limiting (or reducing) their overall cost. Further investigations, notably with larger numbers of rows, can be used to provide systematic design rules for advanced tube-bundle configurations.

Nomenclature

A	SST model constant
c_p	Air specific heat capacity (J.kg^{-1}.K^{-1})
c	Constants in the intermittency transport equation
d	Diameter (m)
$\bar{d}$	Scaled diameter
e	Total specific energy (J.kg^{-1})
E	Destruction terms in SST model
Eu	Euler number
$F_1, F_2,$	Blending functions in SST mode
F_{length}	Empirical correlation to control the length of the transition region
h	Air-side heat transfer coefficient (W.m^{-2}.K^{-1})
k	Thermal conductivity (W.m^{-1}.K^{-1})
$\dot{m}$	Air mass flow rate (kg.s^{-1})
Nu	Nusselt number
P	Pressure (Pa)
ΔP	Pressure drop (Pa)
$\overline{\Delta P}$	Scaled pressure drop.
$P_{\gamma,1}, P_{\gamma,2}$	Production terms in SST model
q	Average heat flux (W.m^{-2})
$\bar{q}$	Scaled average heat flux
Q	Total air-side heat transfer (W)
$\bar{Q}$	Scaled total heat transfer rate
R	Specific gas constant (J.kg^{-1}.K^{-1})
S	Strain rate magnitude (s^{-1})
ΔS	Entropy change rate (W.K^{-1})
S_f	Fin pitch (m)
S_g	Entropy generation rate (W.K^{-1})
S_t	Tube transverse pitch (m)
Re	Reynolds Number
$\bar{S}_g$	Scaled entropy generation
T	Temperature (K)
u	Velocity (m.s^{-1})
W	Weight (kg)
$\bar{W}$	Scaled weight
x_i	Spatial coordinates (m)
Δy	First-to-second cell distance off the wall (m)
y^+	Dimensionless wall distance

Greek characters

α	SST model constant
β	SST model constants
γ	Damping function
δ	Fin thickness (m)
Θ	Scaled approach temperature

κ	Turbulent kinetic energy ($m^2.s^{-2}$)
μ	Air dynamic viscosity (Pa.s)
Π	Intermittency adjunct function
ρ	Air density ($kg.m^{-3}$)
σ	Prandtl-number-like diffusion parameters
τ	Shear stress (Pa)
ω	Specific turbulence dissipation rate (s^{-1})

Subscripts

1, 2, 3, 4	Fin-row index
c	Circular
eff	Effective
f	Fin
g	Generation
i,j	Spatial dimensions indices
in	Inlet
max	Maximum
ot	Outer tube
out	Outlet
t	Turbulent
w	Wall

References

[1] Alta D., Bilgili E., Ertekin C., Yaldiz O., Experimental investigation of three different solar air heaters: energy and exergy analyses, Applied Energy, 87 (2010) 2953-2973.

[2] Zukowski M., Experimental investigations of thermal and flow characteristics of a novel microjet air solar heater, Applied Energy, 142 (2015) 10-20.

[3] Zheng W., Zhang H., You S., Fu Y., Zheng X., Thermal performance analysis of a metal corrugated packing solar air collector in cold regions, Applied Energy, 203 (2017) 938-947.

[4] Hosseini S.S., Ramiar A., Ranjbar A.A., The effect of fins shadow on natural convection solar air heater, International Journal of Thermal Sciences, 142 (2019) 280-294.

[5] Nada S., Said M., Effects of fins geometries, arrangements, dimensions and numbers on natural convection heat transfer characteristics in finned-horizontal annulus, International Journal of Thermal Sciences, 137 (2019) 121-137.

[6] Huang P., Sun Y., A clustering based grouping method of nearly zero energy buildings for performance improvements, Applied Energy, 235 (2019) 43-55.

[7] Lu Y., Zhang X.-P., Huang Z., Lu J., Wang D., Impact of introducing penalty-cost on optimal design of renewable energy systems for net zero energy buildings, Applied Energy, 235 (2019) 106-116.

[8] Gori F., Mascia M., Petracci I., Air cooling of a finned cylinder with slot jets of different height, International Journal of Thermal Sciences, 50 (2011) 1583-1593.

[9] Diani A., Mancin S., Zilio C., Rossetto L., An assessment on air forced convection on extended surfaces: Experimental results and numerical modeling, International Journal of Thermal Sciences, 67 (2013) 120-134.

[10] Shah R.K., Sekulic D.P., Fundamentals of heat exchanger design, John Wiley & Sons, 2003.

[11] Acosta-Iborra A., Campo A., Approximate analytic temperature distribution and efficiency for annular fins of uniform thickness, International Journal of Thermal Sciences, 48 (2009) 773-780.

[12] Senapati J.R., Dash S.K., Roy S., 3D numerical study of the effect of eccentricity on heat transfer characteristics over horizontal cylinder fitted with annular fins, International Journal of Thermal Sciences, 108 (2016) 28-39.

[13] Neal S., Hitchcock J., A study of the heat transfer processes in banks of finned tubes in cross flow, using a large scale model technique, in: pp 290-8 of Proceedings of the Third International Heat Transfer Conference, Chicago, Illinois, August 7-12, 1966. Volume III. New York, American Institute of Chemical Engineers, 1966., Central Electricity Research Labs., Leatherhead, Eng., 1967.

[14] Sung H.J., Yang J.S., Park T.S., Local convective mass transfer on circular cylinder with transverse annular fins in crossflow, International Journal of Heat and Mass Transfer, 39 (1996) 1093-1102.

[15] Chen H.T., Hsu W.L., Estimation of heat-transfer characteristics on a vertical annular circular fin of finned-tube heat exchangers in forced convection, Int. J. Heat Mass. Tran., 51 (2008) 1920-1932.

[16] Bilir L., İlken Z., Erek A., Numerical optimization of a fin-tube gas to liquid heat exchanger, International Journal of Thermal Sciences, 52 (2012) 59-72.

[17] Banerjee R.K., Karve M., Ha J.H., Lee D.H., Cho Y.I., Evaluation of enhanced heat transfer within a four row finned tube array of an air cooled steam condenser, Numerical Heat Transfer, Part A: Applications, 61 (2012) 735-753.

[18] Pongsoi P., Promoppatum P., Pikulkajorn S., Wongwises S., Effect of fin pitches on the air-side performance of L-footed spiral fin-and-tube heat exchangers, International Journal of Heat and Mass Transfer, 59 (2013) 75-82.

[19] Liu J., Jiang Y., Wang B., He S., Assessment and optimization assistance of entropy generation to air-side comprehensive performance of fin-and-flat tube heat exchanger, International Journal of Thermal Sciences, 138 (2019) 61-74.

[20] Yu L.T., Chen C.K., Optimization of circular fins with variable thermal parameters, Journal of the Franklin Institute, 336 (1999) 77-95.

[21] Arslanturk C., Simple correlation equations for optimum design of annular fins with uniform thickness, Applied Thermal Engineering, 25 (2005) 2463-2468.

[22] Kang H.S., Look Jr D., Optimization of a thermally asymmetric convective and radiating annular fin, Heat transfer engineering, 28 (2007) 310-320.

[23] Dhar P., Arora C., Optimum design of finned surfaces, Journal of the Franklin Institute, 301 (1976) 379-392.

[24] Kundu B., Das P., Performance analysis and optimization of annular fin with a step change in thickness, Journal of heat transfer, 123 (2001) 601-604.

[25] Deka A., Datta D., Geometric Size Optimization of Annular Step Fin Using Multi-Objective Genetic Algorithm, Journal of Thermal Science and Engineering Applications, 9 (2017) 021013.

[26] Nemati H., Samivand S., Numerical Study of Flow Over Annular Elliptical Finned Tube Heat Exchangers, Arabian Journal for Science and Engineering, 41 (2016) 4625-4634.

[27] Kundu B., Das P., Performance analysis and optimization of elliptic fins circumscribing a circular tube, International Journal of Heat and Mass Transfer, 50 (2007) 173-180.

[28] Nemati H., Samivand S., Simple correlation to evaluate efficiency of annular elliptical fin circumscribing circular tube, Arabian Journal for Science and Engineering, 39 (2014) 9181-9186.

[29] Nemati H., Samivand S., Performance optimization of annular elliptical fin based on thermo-geometric parameters, Alexandria Engineering Journal, 54 (2015) 1037-1042.

[30] Duffin R.J., McLain D.K., Optimum shape of a cooling fin on a convex cylinder, Journal of Mathematics and Mechanics, (1968) 769-784.

[31] Duffin R., A variational problem relating to cooling fins, Journal of Mathematics and Mechanics, (1959) 47-56.

[32] Arauzo I., Campo A., Cortés C., Quick estimate of the heat transfer characteristics of annular fins of hyperbolic profile with the power series method, Applied Thermal Engineering, 25 (2005) 623-634.

[33] Smith E., Gunter A., Victory S., Fin tube performance, CEP, 62 (1966) 57-67.

[34] Lee D.H., Jung J.M., Ha J.H., Cho Y.I., Improvement of heat transfer with perforated circular holes in finned tubes of air-cooled heat exchanger, International Communications in Heat and Mass Transfer, 39 (2012) 161-166.

[35] Fin Tube Products, Inc. http://www.fintube.com/finbraze-tubing.html.

[36] Hall S., Rules of thumb for chemical engineers, Butterworth-Heinemann, 2017.

[37] Mukherjee R., Effectively design air-cooled heat exchangers, Chemical engineering progress, 93 (1997).

[38] Nemati H., Moghimi M., Numerical study of flow over annular-finned tube heat exchangers by different turbulent models, CFD Letters, 6 (2014) 101-112.

[39] Menter F.R., Two-equation eddy-viscosity turbulence models for engineering applications, AIAA journal, 32 (1994) 1598-1605.

[40] ANSYS/Fluent User Guide version 18.1, ANSYS Incorporated, (2018).

[41] Abraham J., Sparrow E., Tong J., Heat transfer in all pipe flow regimes: laminar, transitional/intermittent, and turbulent, International Journal of Heat and Mass Transfer, 52 (2009) 557-563.

[42] Abraham J., Sparrow E., Minkowycz W., Internal-flow Nusselt numbers for the low-Reynolds-number end of the laminar-to-turbulent transition regime, International Journal of Heat and Mass Transfer, 54 (2011) 584-588.

[43] Gianolio E., Cuti F., Heat transfer coefficients and pressure drops for air coolers with different numbers of rows under induced and forced draft, Heat Transfer Engineering, 3 (1981) 38-48.

[44] Deb K., Multi-objective optimization using evolutionary algorithms, John Wiley & Sons, 2001.

[45] Sacks J., Welch W.J., Mitchell T.J., Wynn H.P., Design and analysis of computer experiments, Statistical science, (1989) 409-423.

[46] Moghimi M., Craig K., Meyer J.P., Optimization of a trapezoidal cavity absorber for the Linear Fresnel Reflector, Solar Energy, 119 (2015) 343-361.

[47] Moghimi M., Craig K., Meyer J.P., Simulation-based optimisation of a linear Fresnel collector mirror field and receiver for optical, thermal and economic performance, Solar Energy, 153 (2017) 655-678.

[48] Moghimi M., Ahmadi G., Wind barriers optimization for minimizing collector mirror soiling in a parabolic trough collector plant, Applied Energy, 225 (2018) 413-423.

[49] Kadivar M., Moghimi M., Sapin P., Markides C., Annulus eccentricity optimisation of a phase-change material (PCM) horizontal double-pipe thermal energy store, Journal of Energy Storage, 26 (2019) 101030.

[50] Ardekani M.M., Optical, thermal and economic optimisation of a linear Fresnel collector, in, University of Pretoria, 2017.

[51] Design Exploration User Guide, version 18.1, ANSYS Incorporated, (2018).